Journal of Sound and Vibration (2002) **257**(4), 615–634
doi:10.1006/jsvi.5058, available online at http://www.idealibrary.com on IDEAL®

A FREQUENCY-DOMAIN METHOD OF STRUCTURAL DAMAGE IDENTIFICATION FORMULATED FROM THE DYNAMIC STIFFNESS EQUATION OF MOTION

U. Lee and J. Shin

Department of Mechanical Engineering, Inha University, 253 *Yonghyun-Dong, Nam-Ku, Incheon* 402-751, *Korea. E-mail*: *ulee@inha.ac.kr*

(*Received* 20 *August* 2001, *and in final form* 10 *December* 2001)

This paper introduces a frequency-domain method of structural damage identification. It is formulated in a general form from the dynamic stiffness equation of motion for a structure and then applied to a beam structure. Only the dynamic stiffness matrix for the intact state appears in the final form of the damage identification algorithm as the structure model. The appealing features of the present damage identification method are: (1) it requires only the frequency response functions experimentally measured from the damaged structure as the input data, and (2) it can locate and quantify many local damages at the same time. The feasibility of the present damage identification method is tested through some numerically simulated damage identification analyses and then experimental verification is conducted for a cantilevered beam with damage caused by introducing three slots.

1. INTRODUCTION

The existence of structural damage within a structure may lead to changes in the dynamic characteristics of the structure such as vibration response, natural frequency, mode shape and modal damping, which, in turn, can be used to detect, locate and quantify the damage. Thus, a number of structural damage identification methods (SDIMs) have appeared in the literature.

The existing SDIMs can be classified into some groups depending on what experimental data are used in the methods. They include: changes in the modal data such as natural frequencies [1], mode shapes [2], and damping ratios [3]; strain energy [4]; transfer function parameters [5]; flexibility matrix [6]; residual forces [7]; wave characteristics [8]; mechanical impedances [9]; and FRF-data [10]. As discussed by Banks *et al.* [11], the modal-data-based SDIMs may have some shortcomings: the modal data are indirectly measured test data and they could be contaminated by measurement errors as well as modal extraction errors. Furthermore, the completeness of modal data cannot be met in most practical cases because they often require a large number of sensors. It can be found from a thorough literature survey that most SDIMs have been derived from finite element method (FEM)-based eigenvalue problems. As a drawback of FEM, very fine meshes should be used to obtain satisfactory dynamic solutions, especially at high frequency. Thus, it is desirable to develop an SDIM by which the shortcomings incurred by the use of modal data and the finite element model can be overcome.

The FRF-data and the spectral element model can be considered as alternatives to the modal data and the finite element model, respectively. Because the FRF-data are measured

0022-460X/02/$35.00

directly from structures, they will be free from errors such as modal extraction errors. Therefore, the FRF-data seem to be more reliable than modal data. A major advantage of using FRF-data over modal data is that the FRF-data can provide much more damage information in a desired frequency range than modal data because the modal data are extracted mainly from a very limited number of FRF-data around resonance [12]. In contrast to the classical FEM, the spectral element method (SEM) is often justifiably referred to as an exact analysis method in the literature [13, 14] because it provides extremely accurate dynamic solutions. The *exact* dynamic element stiffness matrix, often called "spectral element matrix" in the literature, is used in SEM. The *exact* dynamic element stiffness matrix is formulated from the frequency-dependent exact shape functions satisfying governing equations. Because the dynamic element stiffness matrices are stiffness formulated, they can be assembled in a completely analogous way to that used for the conventional FEM to form the dynamic stiffness matrix (DSM) for a complete structure. The difference is that it is done as part of the do-loop over all the frequency components.

In this paper, motivated by the above beautiful features of FRF-data and the exactness of SEM, a frequency-domain method of structural damage identification is derived from the dynamic stiffness equation of motion of a structure and then applied to beam structures. In the present SDIM, the externally applied excitation forces and the FRF-data measured from the damaged structure are used as the input data.

2. DAMAGE IDENTIFICATION ALGORITHM

The dynamics of a structure in the intact state can be represented by the dynamic stiffness equation of motion as [14]

$$[\mathbf{S}(\omega)]\{\mathbf{U}(\omega)\} = \{\mathbf{P}(\omega)\}, \tag{1}$$

where $[\mathbf{S}]$ and $\{\mathbf{U}\}$ are the dynamic stiffness matrix and the spectral components of nodal degrees-of-freedom vector (simply, nodal d.o.f.s) of the structure in the intact state respectively. Note that the dynamic stiffness matrix $[\mathbf{S}]$ is frequency-dependent. The vector $\{\mathbf{P}\}$ represents the spectral components of the externally applied nodal forces vector (simply, nodal forces).

Now, assume that the same structure gets damaged, but still subjected to the same nodal forces as in equation (1). Then, the dynamics of the structure in a damaged state can be represented by

$$[\bar{\mathbf{S}}(\omega)]\{\bar{\mathbf{U}}(\omega)\} = \{\mathbf{P}(\omega)\}, \tag{2}$$

where $[\bar{\mathbf{S}}]$ and $\{\bar{\mathbf{U}}\}$ are the dynamic stiffness matrix and nodal d.o.f.s vector of the structure in a damaged state respectively.

In this study, the matrix $[\mathbf{S}]$ is considered as the known quantity because it is so determined that equation (1) represents the *refined* structure model for the intact structure. By the word "refined", we mean that the experimentally measured and analytically predicted structural dynamics characteristics are in good agreement. Similarly, the vector $\{\bar{\mathbf{U}}\}$ is also considered as a known quantity because it will be measured directly from the damaged structure. However, the dynamic stiffness matrix in the damaged state $[\bar{\mathbf{S}}]$ is not known in advance because it will depend on the not-yet-known current state of damage.

Assume that the matrix $[\bar{\mathbf{S}}]$ can be expressed by

$$[\bar{\mathbf{S}}(\omega)] = [\mathbf{S}(\omega)] + [\Delta\mathbf{S}(\omega)], \tag{3}$$

where $[\Delta\mathbf{S}]$ is the *perturbed* dynamic stiffness matrix generated by the presence of damage. Substituting equation (3) into equation (2) gives

$$\{\mathbf{P}(\omega)\} - [\mathbf{S}(\omega)]\{\bar{\mathbf{U}}(\omega)\} = [\Delta\mathbf{S}(\omega)]\{\bar{\mathbf{U}}(\omega)\}. \tag{4}$$

The nodal forces vector $\{\mathbf{P}\}$ can be written in partitioned-vector form as

$$\{\mathbf{P}(\omega)\} = \begin{Bmatrix} \mathbf{P}_m(\omega) \\ \mathbf{P}_s(\omega) \end{Bmatrix} = \begin{Bmatrix} \mathbf{F}(\omega) \\ \mathbf{0} \end{Bmatrix}, \tag{5}$$

where $\{\mathbf{0}\}$ designates the zero vector. Then, in a manner compatible with equation (5), the vector $\{\bar{\mathbf{U}}\}$ can be partitioned into a set $\{\bar{\mathbf{U}}_m\}$ termed "master" nodal d.o.f.s, which are to be retained, and a set $\{\bar{\mathbf{U}}_s\}$ termed "slave" nodal d.o.f.s, which are to be eliminated to reduce the number of nodal d.o.f.s, as follows:

$$\{\bar{\mathbf{U}}(\omega)\} = \begin{Bmatrix} \bar{\mathbf{U}}_\mathbf{m}(\omega) \\ \bar{\mathbf{U}}_\mathbf{s}(\omega) \end{Bmatrix}. \tag{6}$$

Similarly, the matrices $[\mathbf{S}]$ and $[\bar{\mathbf{S}}]$ can be partitioned as follows:

$$[\mathbf{S}(\omega)] = \begin{bmatrix} \mathbf{S}_{mm}(\omega) & \mathbf{S}_{ms}(\omega) \\ \mathbf{S}_{sm}(\omega) & \mathbf{S}_{ss}(\omega) \end{bmatrix}, \qquad [\bar{\mathbf{S}}(\omega)] = \begin{bmatrix} \bar{\mathbf{S}}_{mm}(\omega) & \bar{\mathbf{S}}_{ms}(\omega) \\ \bar{\mathbf{S}}_{sm}(\omega) & \bar{\mathbf{S}}_{ss}(\omega) \end{bmatrix} \tag{7}$$

Then it follows that

$$[\Delta\mathbf{S}(\omega)] = [\bar{\mathbf{S}}(\omega)] - [\mathbf{S}(\omega)] = \begin{bmatrix} \bar{\mathbf{S}}_{mm} - \mathbf{S}_{mm} & \bar{\mathbf{S}}_{ms} - \mathbf{S}_{ms} \\ \bar{\mathbf{S}}_{sm} - \mathbf{S}_{sm} & \bar{\mathbf{S}}_{ss} - \mathbf{S}_{ss} \end{bmatrix}. \tag{8}$$

Substituting equations (5), (6), and (7b) into equation (2) may yield the relationship between $\{\bar{\mathbf{U}}\}$ and $\{\bar{\mathbf{U}}_m\}$ as follows:

$$\{\bar{\mathbf{U}}(\omega)\} = [\bar{\mathbf{T}}(\omega)]\{\bar{\mathbf{U}}_m(\omega)\}, \tag{9}$$

where $[\bar{\mathbf{T}}]$ is the "co-ordinates" transformation matrix for the structure in a damaged state, which is defined by

$$[\bar{\mathbf{T}}(\omega)] = \begin{bmatrix} \mathbf{I} \\ \bar{\mathbf{t}}(\omega) \end{bmatrix} \tag{10}$$

with

$$[\bar{\mathbf{t}}(\omega)] = -[\bar{\mathbf{S}}_{ss}]^{-1}[\bar{\mathbf{S}}_{sm}]. \tag{11}$$

In equation (10), $[\mathbf{I}]$ denotes the identity matrix. After a lengthy manipulation, the matrix $[\bar{\mathbf{T}}]$ can be rewritten in terms of $[\mathbf{T}]$ (transformation matrix for the structure in the intact

state) and $[\Delta\mathbf{T}]$ (*perturbed* transformation matrix generated by the presence of damage) as follows:

$$[\bar{\mathbf{T}}(\omega)] = [\mathbf{T}(\omega)] + [\Delta\mathbf{T}(\omega)], \tag{12}$$

where

$$[\mathbf{T}(\omega)] = \begin{bmatrix} \mathbf{I} \\ \mathbf{t}(\omega) \end{bmatrix}, \qquad [\mathbf{t}(\omega)] = -[\mathbf{S}_{ss}]^{-1}[\mathbf{S}_{sm}] \tag{13}$$

and

$$[\Delta\mathbf{T}(\omega)] = \begin{bmatrix} \mathbf{0} \\ \Delta\mathbf{t}(\omega) \end{bmatrix}, \qquad [\Delta\mathbf{t}(\omega)] = [\mathbf{C}_{ss}][\mathbf{t}] + [\mathbf{t}][\mathbf{C}_{sm}] + [\mathbf{C}_{ss}][\mathbf{t}][\mathbf{C}_{sm}], \tag{14}$$

where the following definitions are used:

$$[\mathbf{C}_{ss}] = -[\mathbf{S}_{ss}]^{-1}[\Delta\mathbf{S}_{ss}]([\mathbf{I}] + [\mathbf{S}_{ss}]^{-1}[\Delta\mathbf{S}_{ss}])^{-1}, \tag{15}$$

$$[\mathbf{C}_{sm}] = [\mathbf{S}_{sm}]^{-1}[\Delta\mathbf{S}_{sm}].$$

Substituting equation (12) into equation (9) and its result into equation (4) gives

$$\{\mathbf{P}\} - [\mathbf{S}][\mathbf{T}]\{\bar{\mathbf{U}}_m\} = ([\mathbf{S}][\Delta\mathbf{T}] + [\Delta\mathbf{S}][\mathbf{T}] + [\Delta\mathbf{S}][\Delta\mathbf{T}])\{\bar{\mathbf{U}}_m\}. \tag{16}$$

Applying equations (5), (7a), (8), (13a), and (14a) into equation (16) and then neglecting some small terms may yield

$$\{\mathbf{F}(\omega)\} - [\mathbf{X}(\omega)]\{\bar{\mathbf{U}}_{\mathbf{m}}(\omega)\} = [\mathbf{Y}(\omega)]\{\bar{\mathbf{U}}_{\mathbf{m}}(\omega)\}, \tag{17}$$

where

$$[\mathbf{X}(\omega)] = [\mathbf{S}_{mm}] - [\mathbf{S}_{ms}][\mathbf{S}_{ss}]^{-1}[\mathbf{S}_{sm}] \tag{18}$$

and

$$[\mathbf{Y}(\omega)] = [\mathbf{T}]^{\mathrm{T}}[\Delta\mathbf{S}][\mathbf{T}]. \tag{19}$$

One may note that the effects of damage appear only on the right-hand side of equation (17) through the *perturbed* dynamic stiffness matrix $[\Delta\mathbf{S}]$.

The "inertance" FRF is defined as the ratio of the acceleration to the applied force as [15]

$$A_{mi} \equiv -\omega^2 \frac{\bar{\mathbf{U}}_{mi}}{F_i} \quad \text{or} \quad \{\mathbf{A}_m\} \equiv -\omega^2 \left\{\frac{\bar{\mathbf{U}}_m}{\mathbf{F}}\right\}, \tag{20}$$

where the subscript i denotes the components of the vectors $\{\mathbf{F}\}$, $\{\bar{\mathbf{U}}_m\}$,and $\{\mathbf{A}_m\}$. By using the definition of equation (20), equation (17) can be rewritten as

$$\{\boldsymbol{\delta}\} + \frac{1}{\omega^2}[\mathbf{X}(\omega)]\{\mathbf{A}_m(\omega)\} = -\frac{1}{\omega^2}[\mathbf{Y}(\omega)]\{\mathbf{A}_m(\omega)\}, \tag{21}$$

where $\{\boldsymbol{\delta}\}$ is the nodal forces locator vector, which has unit values only at the components corresponding to non-zero nodal forces.

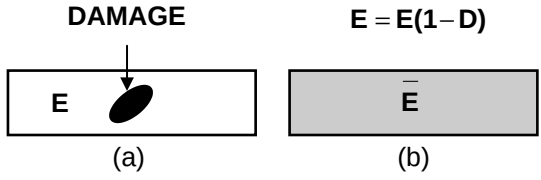

Figure 1. Example of finite structure element with damage: (a) true damage state, and (b) its equivalent representation in terms of effective uniform damage magnitude D.

For a complete intact structure, the dynamic stiffness matrix $[\mathbf{S}]$ can be assembled from the dynamic element stiffness matrices as follows:

$$[\mathbf{S}(\omega)] = \sum_{k=1}^{N} [\mathbf{L}_k]^{\mathrm{T}} [\mathbf{s}_k(\omega)][\mathbf{L}_k], \tag{22}$$

where N is the number of finite elements and $[\mathbf{s}_k]$ is the dynamic element stiffness matrix for the kth element. The matrix $[\mathbf{L}_k]$ is the locator matrix, which locates the components of $[\mathbf{s}_k]$ into $[\mathbf{S}]$ for the assembly. Similarly, the *perturbed* dynamic stiffness matrix $[\Delta\mathbf{S}]$ can be obtained from

$$[\Delta\mathbf{S}(\omega)] = \sum_{k=1}^{N} [\mathbf{L}_k]^{\mathrm{T}} [\Delta\mathbf{s}_k(\omega)][\mathbf{L}_k], \tag{23}$$

where $[\Delta\mathbf{s}_k]$ is the *perturbed* dynamic element stiffness matrix for the kth element. As shown in Figure 1, assume that a small finite structure element having non-uniform damage inside can be represented as the "effective" finite structure element now having uniform damage through the whole structure. Then, the *perturbed* matrix $[\Delta\mathbf{s}_k]$ can be approximately related to $[\mathbf{s}_k]$ as follows:

$$[\Delta\mathbf{s}_k(\omega)] \cong D_k[\mathbf{s}_k(\omega = 0)] = D_k[\mathbf{k}_k], \tag{24}$$

where D_k and $[\mathbf{k}_k]$ are "effective" uniform damage magnitude and conventional finite element stiffness matrix for the kth element, respectively. Numerical verification of equation (24) is given for the beam element in the following section.

By using equations. (19), (23) and (24), the right-hand side of equation (21) can be expressed as

$$-\frac{1}{\omega^2}[\mathbf{Y}(\omega)]\{\mathbf{A}_m(\omega)\} = -\frac{1}{\omega^2}[\mathbf{T}]^{\mathrm{T}}\left(\sum_{k=1}^{N}[\mathbf{L}_k]^{\mathrm{T}}[\mathbf{k}_k][\mathbf{L}_k]D_k\right)[\mathbf{T}]\{\mathbf{A}_m\} \tag{25}$$

or

$$-\frac{1}{\omega^2}[\mathbf{Y}(\omega)]\{\mathbf{A}_m(\omega)\} = [\mathbf{\Phi}(\omega)]\{\mathbf{D}\}, \tag{26}$$

where

$$\begin{aligned}
&[\mathbf{\Phi}(\omega)] = [\boldsymbol{\varphi}_1(\omega)\boldsymbol{\varphi}_2(\omega) \ldots \boldsymbol{\varphi}_N(\omega)],\\
&\{\mathbf{D}\} = \{D_1 D_2 \ldots D_N\}^{\mathrm{T}}\\
&\{\boldsymbol{\varphi}_k(\omega)\} = -\frac{1}{\omega^2}([\mathbf{L}_k][\mathbf{T}(\omega)])^{\mathrm{T}}[\mathbf{k}_k(\omega)]([\mathbf{L}_k][\mathbf{T}(\omega)])\{\mathbf{A}_m(\omega)\}.
\end{aligned} \tag{27}$$

Replacing the right-hand side of equation (21) with that of equation (26) may yield a set of linear algebraic equations in N unknown (effective) damage magnitudes D_k as follows:

$$[\mathbf{\Phi}(\omega)]_{M\times N}\{\mathbf{D}\}_{N\times 1} = \{\mathbf{b}(\omega)\}_{M\times 1}, \tag{28}$$

where

$$\{\mathbf{b}(\omega)\} = \{\boldsymbol{\delta}(\omega)\} + \frac{1}{\omega^2}[\mathbf{X}(\omega)]\{\mathbf{A}_m(\omega)\}. \tag{29}$$

Equations (27) and (29) show that $[\Phi]$ and $\{\mathbf{b}\}$ are determined only from the dynamic stiffness matrix in the intact state $[\mathbf{S}]$, the nodal forces locator vector $\{\boldsymbol{\delta}\}$, and the measured inertance FRF $\{\mathbf{A}_m\}$, and thus equation (28) does not require the dynamic stiffness matrix in the damaged state. The dimension of the matrix $[\Phi]$ is $M \times N$, where M is the number of "master" nodal d.o.f.s $\{\bar{\mathbf{U}}_m\}$ and N is the number of finite elements to be examined for unknown damage magnitudes D_k. Accordingly, the dimension of the nodal forces locator vector $\{\boldsymbol{\delta}\}$ is $M \times 1$.

In equation (6), the nodal d.o.f.s at which neither the nodal forces are applied nor the forced-vibration responses (i.e., inertance FRF) are measured are considered as the "slave" nodal d.o.f.s, whereas the other nodal d.o.f.s are considered as the "master" nodal d.o.f.s. Thus, to vibrate the damaged structure, the nodal forces should be applied only to some of the M nodes at which the forced-vibration responses will be measured. Accordingly, the number of nodal forces is in general less than the number of "master" nodal d.o.f.s M. This requirement can be readily met by applying an excitation force at a single node, for instance, and then by measuring vibration responses at some pre-specified nodes including the node at which the excitation force is applied.

In general, the number of unknown damage magnitudes is much larger than the number of measured nodal d.o.f.s (or the number of linear algebraic equations), i.e., $N > M$. Thus, it is required to derive more linear algebraic equations from equation (28) in order to make the damage identification problem well-posed. Otherwise, the use of a proper optimal solution technique seems inevitable. One may note that equation (28) is valid for any frequency ω. This means that a different set of linear algebraic equations in the same N unknown damage magnitudes D_k can be obtained from equation (28) by properly choosing a different value of frequency ω. Thus, one can vary the excitation frequency ω in order to collect as many different sets of linear algebraic equations as needed to form a system of N linear algebraic equations as follows:

$$[\mathbf{\Psi}]_{N\times N}\{\mathbf{D}\}_{N\times 1} = \{\mathbf{B}\}_{N\times 1}, \tag{30}$$

where

$$[\mathbf{\Psi}]_{N\times N} = \begin{bmatrix} [\mathbf{\Phi}(\omega_1)]_{M\times N} \\ [\mathbf{\Phi}(\omega_2)]_{M\times N} \\ \vdots \\ [\mathbf{\Phi}(\omega_q)]_{M\times N} \end{bmatrix} \tag{31}$$

and

$$\{\mathbf{B}\}_{N\times 1} = \begin{Bmatrix} \{\mathbf{b}(\omega_1)\}_{M\times 1} \\ \{\mathbf{b}(\omega_2)\}_{M\times 1} \\ \vdots \\ \{\mathbf{b}(\omega_q)\}_{M\times 1} \end{Bmatrix} \tag{32}$$

where $N = q \times M$. Equation (30) can be solved for N unknown damage magnitudes D_k in N finite elements, which implies the location and quantification of many local damages.

In summary, equation (30) represents an SDIM newly developed in this study. The appealing features of the present SDIM are as follows:

(1) It is formulated from the dynamic stiffness equation of motion.
(2) It requires the dynamic stiffness matrix only for the intact state.
(3) It requires the forced-vibration responses (i.e., the inertance FRF) of the damaged structure only as the input data.
(4) It can locate and quantify many local damages simultaneously.

3. APPLICATION TO THE BEAM STRUCTURE

3.1. EFFECTIVE DAMAGE MAGNITUDE

Consider a finite beam element having local damages inside, as shown in Figure 1(a). Because the location, geometry, and the severity of the damage are not known in advance for most practical cases, it is almost impossible to assign a definitive representation for the stiffness at the site of damage. Thus, as shown in Figure 1(b), a simple, but rational approach [11, 16, 17] is to represent the presence of damage by the degradation of Young's modulus as follows:

$$\bar{E} = E(1 - D), \tag{33}$$

where E and $\bar{E}$ are the Young's moduli for the intact and damaged states, respectively, and D is the effective uniform damage magnitude through the whole element. The case $D = 0$ indicates the intact state, while $D = 1$ indicates the complete rupture of material due to damage.

It is known that damages may give rise to certain non-linearities, for example, clearance or bilinear stiffness effects in systems with cracks. Most damages before the structural failure are localized at very small spots within a structure rather than spread wide over the structure. Furthermore, if the local damages are weak, the non-linearities will be very weak and their effects will be confined to the zones very near the local damages. Thus, for most local damages that are weak at the early stage of growth, one may assume that their non-linearities can be neglected or, if needed, can be included into the effective damage magnitude of equation (33) as the equivalent linearized effects.

3.2. DYNAMIC ELEMENT STIFFNESS MATRIX

The exact dynamic element stiffness matrix for an intact finite Bernoulli–Euler beam element is given by [13, 14]

$$[\mathbf{s}(\omega)] = \frac{\kappa EI}{Ch\, c - 1} \begin{bmatrix} \mathbf{s}_1 & \mathbf{s}_2 \\ \mathbf{s}_2^{\mathrm{T}} & \mathbf{s}_3 \end{bmatrix} \tag{34}$$

with

$$[\mathbf{s}_1] = \begin{bmatrix} -\kappa^2(Ch\,s + Sh\,c) & -\kappa Sh\,s \\ -\kappa Sh\,s & -(Ch\,s - Sh\,c) \end{bmatrix},$$

$$[\mathbf{s}_2] = \begin{bmatrix} \kappa^2(Sh + s) & -\kappa(Ch - c) \\ \kappa(Ch - c) & -(Sh - s) \end{bmatrix} \tag{35}$$

$$[\mathbf{s}_3] = \begin{bmatrix} -\kappa^2(Ch\,s + Sh\,c) & \kappa Sh\,s \\ \kappa Sh\,s & -(Ch\,s - Sh\,c) \end{bmatrix},$$

where

$$\begin{aligned} s &= \sin \kappa l, \qquad c = \cos \kappa l, \\ Sh &= \sinh \kappa l, \quad Ch = \cosh \kappa l \end{aligned} \tag{36}$$

where EI and l are the bending stiffness and length of the beam element, respectively, and κ is the wave number. The exact dynamic element stiffness matrix for a damaged Bernoulli–Euler beam element can be reduced from equation (34) by simply replacing E with $\bar{E} = E(1 - D)$ as follows:

$$[\bar{\mathbf{s}}(\omega; D)] = [\mathbf{s}(\omega)]_{E = \bar{E}} \tag{37}$$

Subtracting $[\bar{\mathbf{s}}]$ from $[\mathbf{s}]$ yields the *exact* perturbed dynamic element stiffness matrix as

$$[\Delta\mathbf{s}(\omega)]_{exact} = [\bar{\mathbf{s}}(\omega)] - [\mathbf{s}(\omega)]. \tag{38}$$

Expanding $[\Delta s]_{exact}$ in the Taylor series with respect to D and neglecting the higher order terms may yield the *approximated* perturbed dynamic element stiffness matrix as follows:

$$[\Delta\mathbf{s}(\omega)]_{approx} \cong D[\mathbf{s}(\omega = 0)] = D[\mathbf{k}], \tag{39}$$

where $[\mathbf{k}]$ is the conventional finite element stiffness matrix for the finite Bernoulli–Euler beam element [18].

The percent errors of the components of $[\Delta\mathbf{s}]_{approx}$ with respect to those of $[\Delta\mathbf{s}]_{xa}$ are illustrated in Figure 2 when the uniform damage magnitude is $D = 0{\cdot}4$ and the length-to-thickness ratio of the beam element is $l/h = 9$. Figure 2 shows that the components $\Delta\mathbf{s}_{11approx}$ and $\Delta\mathbf{s}_{33approx}$ are equal in magnitude and in general have the largest percent error. Thus, the percent errors of $\Delta\mathbf{s}_{11approx}$ are further detailed in Figure 3 for different length-to-thickness ratios and uniform damage magnitudes. Figure 3 shows that, once the maximum frequency range of measured inertance FRF to be used for damage identification is determined, the accuracy of $[\Delta\mathbf{s}]_{approx}$ can be improved by reducing the length-to-thickness ratio of the beam element, in other words, by shortening the beam element. The approximated perturbed dynamic element stiffness $[\Delta\mathbf{s}]_{approx}$ given by equation (39) is adopted in the present study because it is linear in the effective uniform damage magnitude D and because its accuracy can be readily improved by properly choosing both the length-to-thickness ratio of the beam element and the maximum frequency range of measured inertance FRF to be used for damage identification.

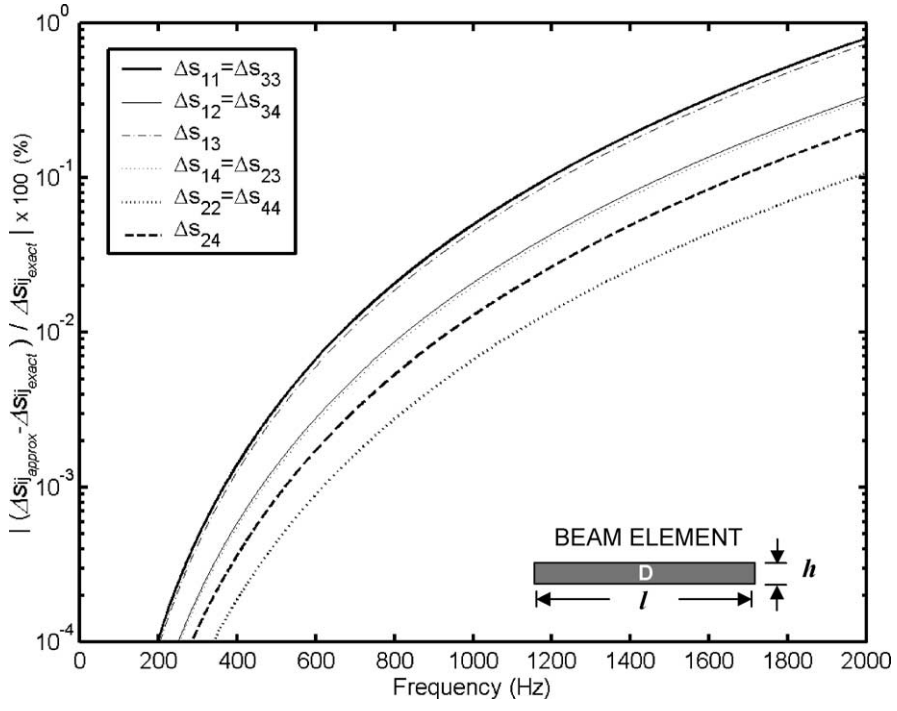

Figure 2. Percent errors of the components of $[\Delta \mathbf{s}]_{approx}$ with respect to those of $[\Delta \mathbf{s}]_{exact}$ for the Bernoulli-Euler beam element: $l/h = 9$ and $D = 0{\cdot}4$.

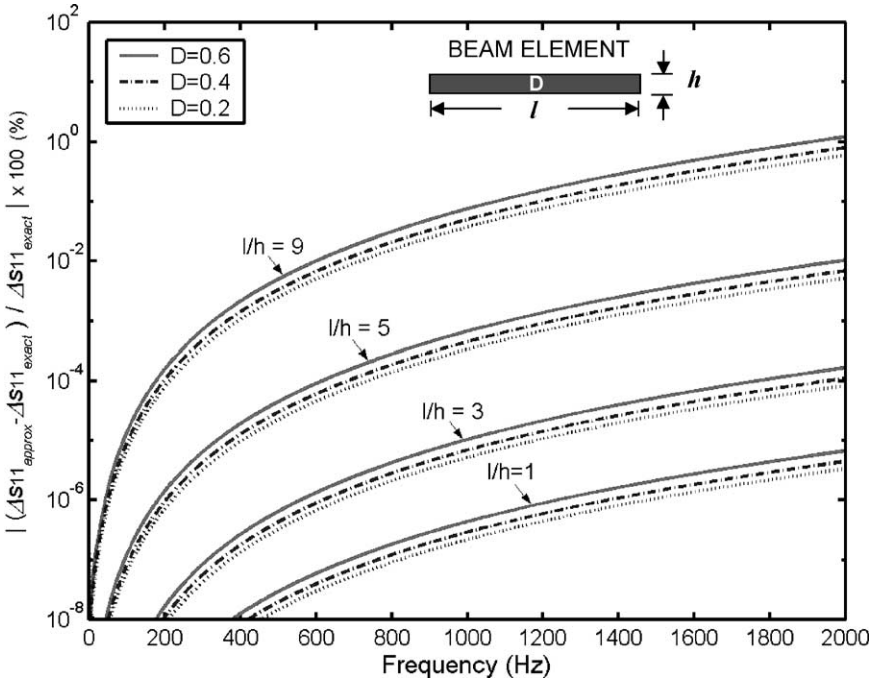

Figure 3. Percent errors of $\Delta \mathbf{s}_{11approx}$ with respect to $\Delta \mathbf{s}_{11exac}$ for the Bernoulli–Euler beam element depending on the length-to-thickness ratio (l/h) and uniform damage magnitude (D).

4. NUMERICAL AND EXPERIMENTAL VERIFICATIONS

4.1. NUMERICALLY SIMULATED TESTS

Before conducting experimental verification, first the feasibility of the present SDIM was evaluated through some numerically simulated damage identification tests. For the feasibility tests, first the pre-specified damages are placed in a beam and then inversely identified by using the present SDIM. Figure 4 shows the locations and magnitudes of three piece-wise uniform damages (i.e., $D_1 = 0{\cdot}4$, $D_2 = 0{\cdot}5$, and $D_3 = 0{\cdot}3$) placed on a cantilevered aluminum beam considered for the feasibility tests. The beam has the length $L = 0{\cdot}4$ *m*, the bending stiffness $EI = 14{\cdot}6\ \mathrm{N\,m^2}$, and the mass density per length $\rho A = 0{\cdot}275$ kg/m. The bending stiffness and mass density are experimentally measured. In Figure 4, the circle ($\bigcirc$) indicates the location of the excitation point and the crosses ($\times$) indicate the three FRF measurement points. Analytically predicted FRFs are used for the numerically simulated damage identification tests, and they are calculated at $x = 0{\cdot}133$, $0{\cdot}267$, and $0{\cdot}356$ m by applying a harmonic point force at $x = 0{\cdot}133$ m.

In real situations, the inertance FRFs required in equation (28) should be experimentally measured directly from a damaged structure. Thus, in practice, they are liable to be contaminated by certain measurement noises. Thus, by following the approach used by Thyagarajan *et al.* [10], an e% random noise is added to the analytically predicted FRF to represent the errors in measured FRF data:

$$\bar{\mathbf{A}} = \mathbf{A}\left(1 + \frac{e}{100} \times randn\right), \tag{40}$$

where $\mathbf{A}$ and $\bar{\mathbf{A}}$ denote the inertance FRFs before and after the e% random noise is taken into account, and "*randn*" represents the random noise generator function in MATLAB®. As done by Thyagarajan *et al.* [10], it is assumed that the random noise is uniformly distributed, with the mean = 0 and variance = 1.

In this study, the accuracy of the predicted damage with respect to the actual value is evaluated by using the "damage identification error (DIE)" defined by

$$DIE \equiv \sqrt{\frac{1}{L}\sum_{j}^{\mathrm{N}} l_j (D_j^{Pred} - D_j^{True})^2}, \tag{41}$$

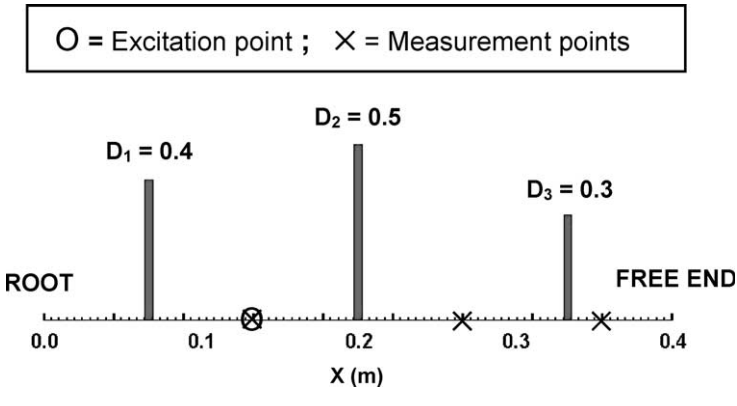

Figure 4. Cantilevered beam with three piece-wise uniform damages considered for numerically simulated damage identification tests.

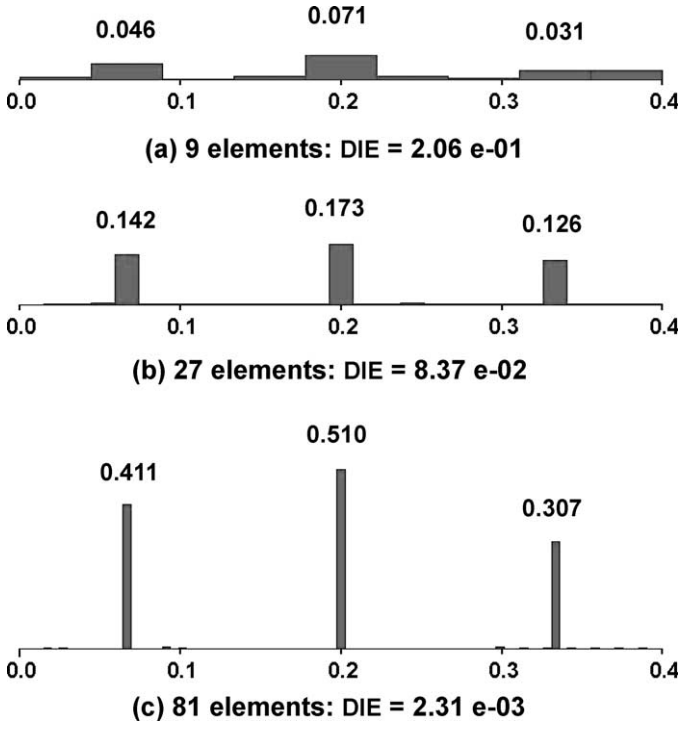

Figure 5. Analytically predicted FRF-data-based damage identification results depending on the number of finite elements used in the analysis: 0% random noise in FRF.

where L is the total length of the beam, and D_j is the effective damage magnitude for the jth beam element of length l_j. The superscripts "*True*" and "*Pred*" denote the true and predicted damages respectively. As the value of DIE becomes smaller, the predicted damages become closer to the true values.

Figure 5 shows the numerically simulated damage identification results for 0% random noise in FRF. The beam is divided into nine equal finite elements at the first iteration, and 27 equal finite elements at the second iteration, and so on. Because three FRF measurement points are chosen for the present example case (see Figure 4), three excitation frequencies are used to obtain a total of nine equations for the nine finite elements model at the first iteration (see Figure 5(a))—similarly, nine and 27 excitation frequencies for the 27 and 81 finite elements models at the second and third iterations (see Figures 5(b) and 5(c)) respectively. How to choose those excitation frequency points may play an important role for the successful damage identification, which was discussed by the present authors in their previous work [19]. In the authors' experiences, it is recommended to choose the excitation frequency points near the resonance peaks in the low-frequency range. As the number of finite elements used in the analysis is increased in this way, Figure 5 certainly shows that the value of DIE decreases and the predicted damages accordingly converge almost to the true values $D_1 = 0{\cdot}4$, $D_2 = 0{\cdot}5$, and $D_3 = 0{\cdot}3$.

Figure 6 shows the accuracy of damage identification depending on the level of random noises in FRF. The results in Figure 6 were obtained from the mean values of five simulations conducted for each level of random noise in FRF. As expected, the accuracy of damage identification falls off gradually as the level of random noises in FRF increases. The

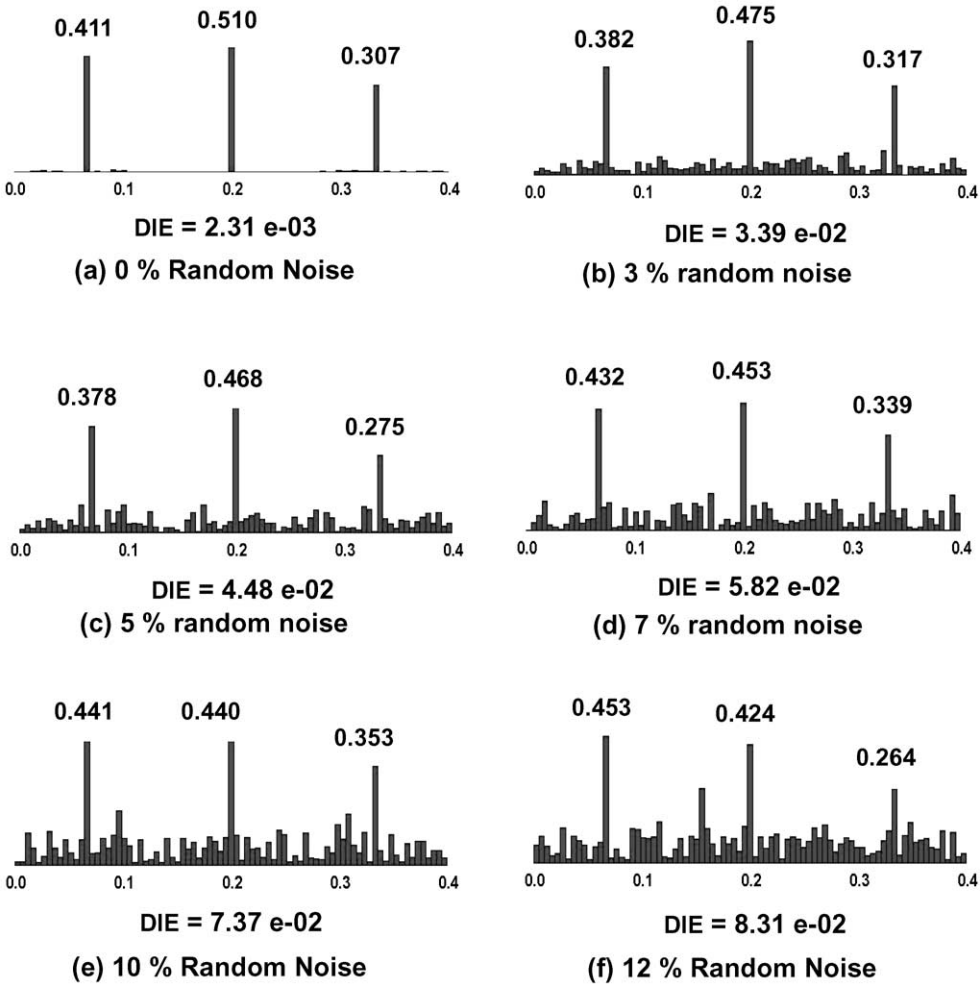

Figure 6. Analytically predicted FRF-data-based damage identification results depending on the level of random noises in FRFs.

present SDIM is found to fairly well locate three pre-specified damages up to about 10% random noise. If the level of random noises in FRF becomes larger than about 12%, then the smallest damage $D_3 = 0{\cdot}3$ cannot be detected well. From Figures 6(e) and 6(d), one may realize that the damage magnitude difference of 0·1 cannot be well quantified if the random noises in FRF are larger than about 5%. Thus, to successfully quantify small and/or weak damages as well as to successfully detect and locate them, it is certainly required to acquire very accurate experimentally measured FRFs.

The advantage of the present SEM-based damage identification method over the FEM-based methods [7, 10, 12] is investigated by comparing the damage identification results obtained by the present SEM- and FEM-based methods. The results by the FEM-based method are obtained from equation (30) by using the approximate dynamic stiffness matrix from classical FEM formulation [18]. As an illustrative problem, a cantilevered beam represented by the 81 equal finite elements model is considered herein. Three piece-wise uniform damages (i.e., $D_1 = 0{\cdot}4$, $D_2 = 0{\cdot}5$, and $D_3 = 0{\cdot}3$) are placed on the

TABLE 1

Damage identification results by the present SEM- and FEM-based methods by varying the length of finite elements

Length of finite element (m)	Identified damage magnitudes (% errors w.r.t. true damage magnitudes)						Damage identification error ($DIE \times 10^{-3}$)	
	D_1		D_2		D_3			
	SEM	FEM	SEM	FEM	SEM	FEM	SEM	FEM
0·8/81	0·404 (1·00%)	0·404 (1·00%)	0·510 (2·00%)	0·510 (2·00%)	0·308 (2·67%)	0·308 (2·67%)	5·156	5·157
1·6/81	0·404 (1·00%)	0·405 (1·25%)	0·512 (2·40%)	0·512 (2·40%)	0·308 (2·67%)	0·309 (3·00%)	8·821	8·824
3·2/81	0·409 (2·25%)	0·411 (2·75%)	0·486 (2·80%)	0·474 (5·20%)	0·308 (2·67%)	0·315 (5·00%)	14·20	21·23
6·4/81	0·409 (2·25%)	0·382 (4·50%)	0·515 (3·00%)	0·530 (6·00%)	0·290 (3·34%)	0·271 (9·67%)	26·52	51·93

14th, 41st, and 68th finite elements of the beam. First, the accuracy of damage identification is compared by varying the length of the finite element. The length of the beam is increased up to 6·4 m to increase the length of the finite element. The exact dynamic stiffness matrix used in the present SEM-based method keeps exact regardless of the length of the finite element. On the other hand, the approximate dynamic stiffness matrix from classical FEM formulation becomes less accurate as the length of the finite element is increased. As a result, Table 1 shows that the FEM-based method provides relatively poor damage identification results when compared with the present SEM-based method. Next, the detectability of small damages is compared by reducing the original magnitudes of damages by $1/N$ (see Figure 7) while keeping the length of the cantilevered beam as 0·4 m. It is very clear from Figure 7 that the present SEM-based method becomes more accurate as the magnitudes of damages get smaller while the FEM-based method becomes less accurate. These interesting results come from the following facts: first, the dynamic stiffness matrix used in the present SEM-based method is exact while that used in the FEM-based method is approximate; second, the error by the use of the *approximated* perturbed dynamic element stiffness matrix (i.e., equation (39)) in the present SEM-based algorithm becomes small as damage magnitudes decrease, which can be observed from Figure 3. This implies that the present SEM-based method can be promisingly applied to identify rather very small damages as far as very accurate FRF-data can be measured from damaged structures, which will be one of important advantages of the present SEM-based method over the existing FEM-based methods.

Though the approximate dynamic stiffness matrix can be also used in the damage identification algorithm developed herein (see Table 1 and Figure 7), the use of the exact dynamic stiffness matrix is mandatory to get more reliable damage identification results. In general, it is quite straightforward to formulate the exact dynamic stiffness matrices for structures such as beams, frames, and trusses; all consist of one-dimensional structure elements. However, it is not true for two- and three-dimensional structures [13, 14]. Thus, the disadvantage of the present SEM-based method will be its applicability that is limited to structures for which exact dynamic stiffness matrices are available.

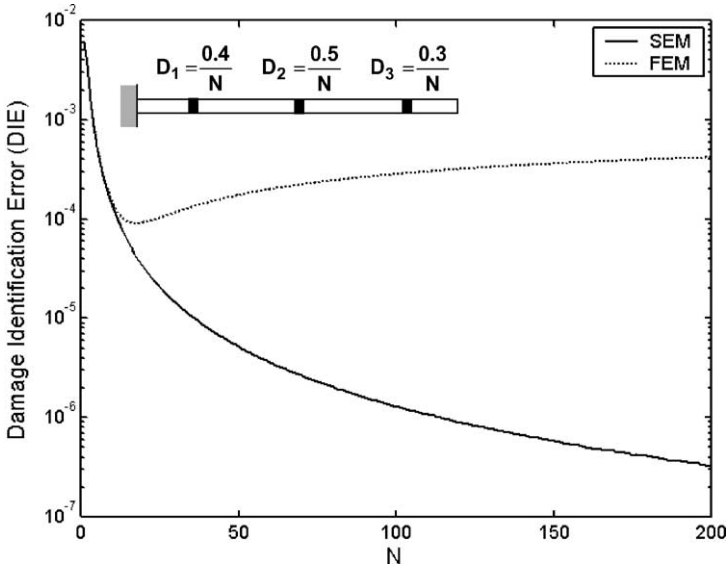

Figure 7. Comparison of damage identification results by the present SEM- and FEM-based methods by varying the magnitudes of damages.

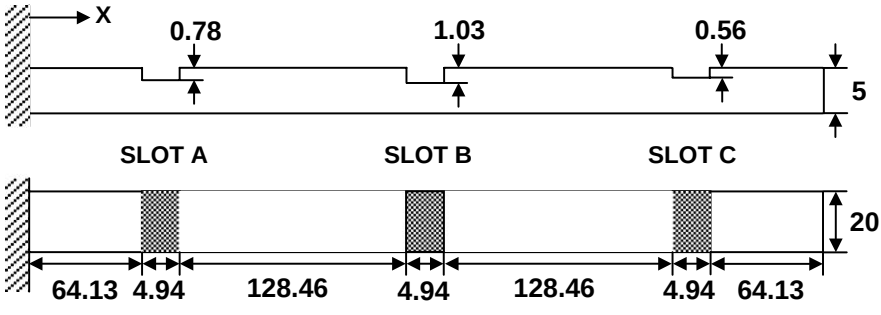

Figure 8. Geometry of a cantilevered beam specimen with three slots (units: mm)

4.2. EXPERIMENTAL TESTS

Figure 8 shows the cantilevered beam specimen used for experiments. The beam is 0·4 m long, 0·02 m wide, and 0·005 m thick. The mass density and bending stiffness for the intact state are obtained by experiments as $\rho A = 0{\cdot}275$ kg/m and $EI = 14{\cdot}6$ N m^2 respectively. The intact beam is damaged by introducing three slots 4·94 mm wide and 0·78, 1·03, and 0·56 mm deep, i.e., slot A, slot B and slot C in Figure 8. The depths of slot A, slot B, and slot C are so determined that the corresponding effective damages become 0·4, 0·5, and 0·3 respectively. To vibrate the beam specimen, an impulse force is applied to the beam specimen by the shaker B&K 4810. The impulse signal is generated by the signal analyzer B&K 2034, and the vibration responses of the beam specimen are measured by using the accelerometer B&K 4374. To measure the FRF with the highest frequency resolution of the signal analyzer HP 35670A, the experiment is repeated for three successive frequency ranges, i.e., first from 0 to 1600 Hz, next from 1600 to 3200Hz, and lastly from 3200 to 4800 Hz, instead of conducting a single experiment for the whole frequency range of interest up to 4800 Hz.

TABLE 2

Experimentally measured natural frequencies of the beam with damage

	Measured natural frequencies (Hz)							
Beams	1st	2nd	3rd	4th	5th	6th	7th	8th
Undamaged	25·75	156·9	438·7	859·3	1419	2117	2949	3915
Damaged	25·01	154·2	435·8	838·4	1397	2066	2931	3860
% Decrease	2·87	1·72	0·67	2·43	1·56	2·39	0·58	1·41

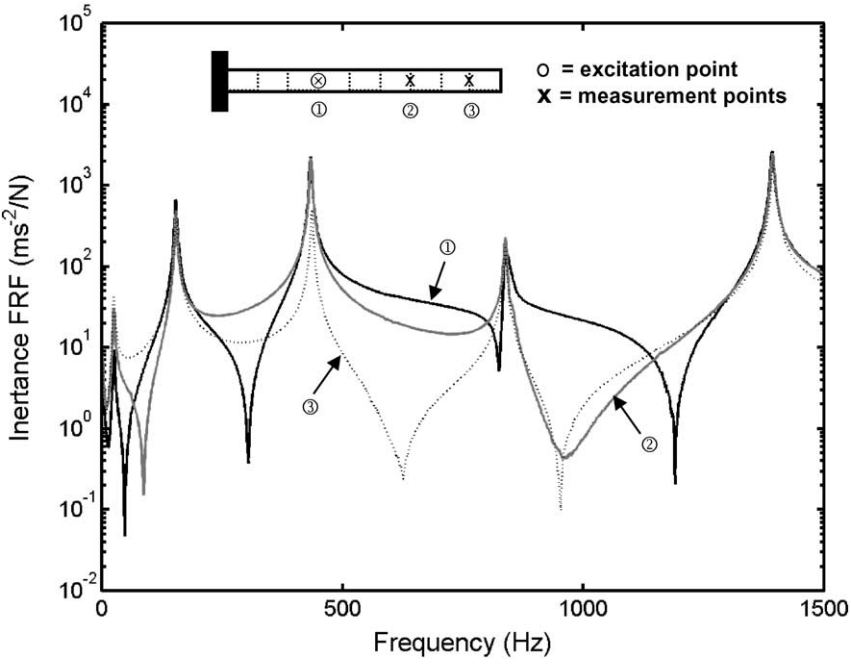

Figure 9. Inertance FRFs measured at $x = 0{\cdot}133$ m (point 1), 0·267 m (point 2), and 0·356 m (point 3) of the damaged beam by applying an impact load at $x = 0{\cdot}133$ m (point 1).

Table 2 compares the natural frequencies of the beam specimen measured before and after damage. It shows that, in general, the damage (i.e., cuts) tends to lower the natural frequencies. Figure 8 shows the inertance FRFs of the damaged beam specimen measured at $x = 0{\cdot}133$ m (point 1), 0·267 m (point 2), and 0·356 m (point 3) by applying an impact load at $x = 0{\cdot}133$ m (point 1). To investigate the effects of damage on the inertance FRF, the inertance FRFs measured at point 1 before and after damage are compared in Figure 10. From Figure 10, one may find that, in general, the damage tends to shift the resonance peaks to the lower frequencies as well as to reduce them in magnitude.

Figure 11 shows the damage identification results obtained by using the experimentally measured inertance FRFs given in Figure 9. One may observe the following. First, as observed in the numerically simulated damage identification (for instance, see Figure 5), the effective damage magnitudes predicted by using the measured inertance FRFs indeed get closer to the actual values as the number of finite elements is increased. Second, when

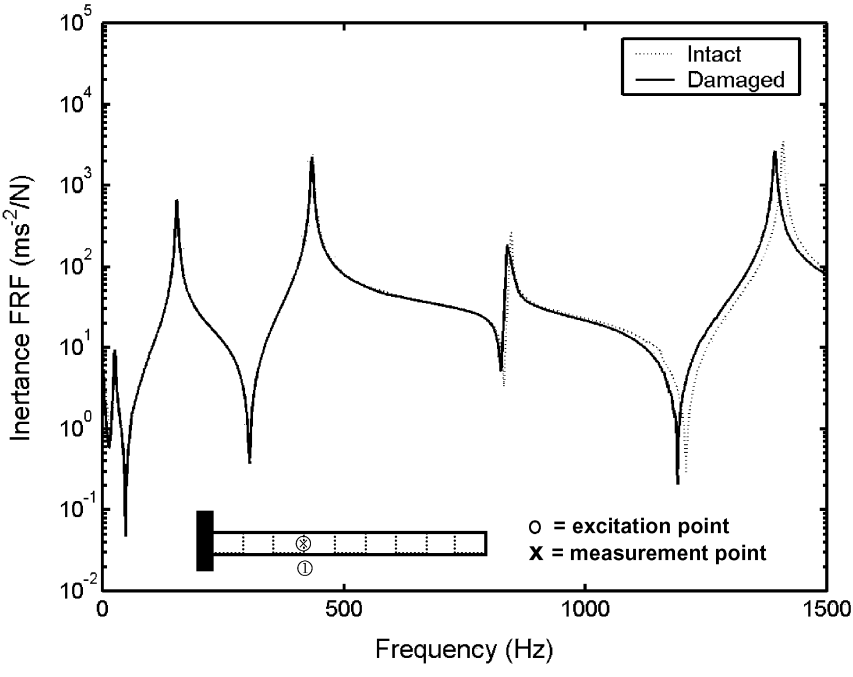

Figure 10. Comparison of the inertance FRFs at intact and damaged states, all measured at $x = 0{\cdot}133$ m (point 1) of the damaged beam by applying an impact load at the same point.

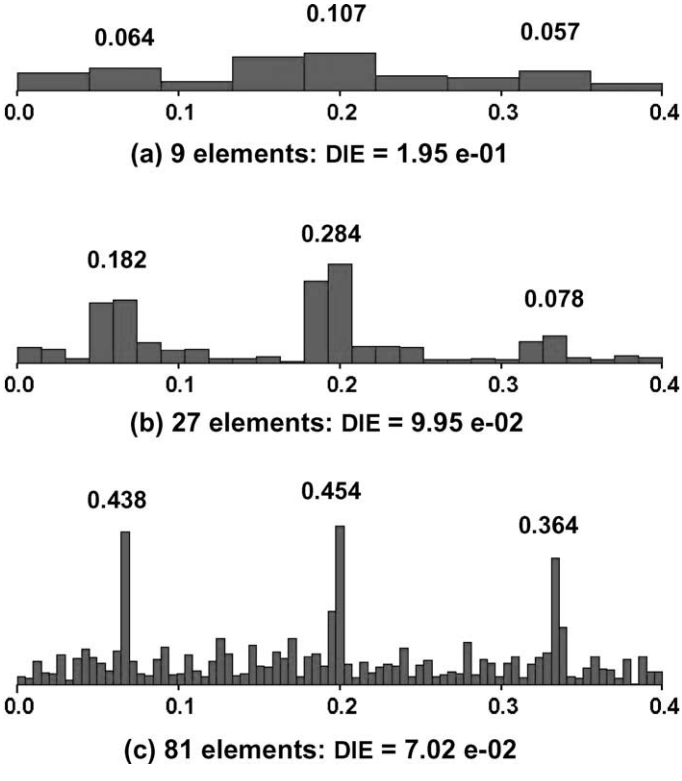

Figure 11. Experimentally measured FRF-data-based damage identification results depending on the number of finite elements used in the analysis.

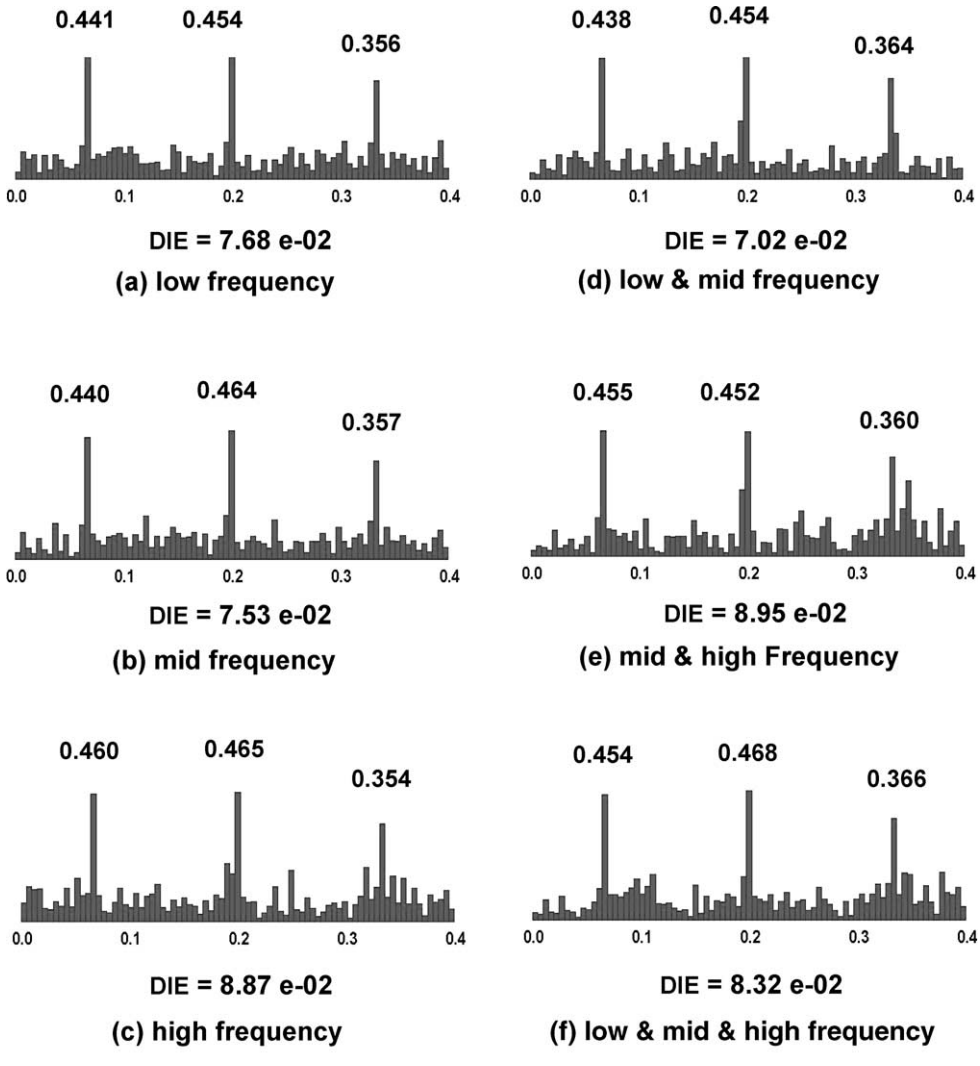

Figure 12. Experimentally measured FRF-data-based damage identification results depending on the frequency range of excitation: low $0 < \omega < 500$ Hz, mid $500 < \omega < 1000$ Hz, high $1000 < \omega < 1500$ Hz.

compared with the case of analytically predicted FRFs with zero random noise (see Figure 5), the experimentally measured FRFs predict incorrect damage magnitudes even over the zone without damage. The result in Figure 11(c) is found to be quite similar to that obtained by assuming 7% random noises in the analytically predicted FRFs, i.e., Figure 6(d). Third, the present SDIM is found to fairly well locate and quantify three slots.

Figure 12 is given to show the effects of the range of excitation frequency on the accuracy of damage identification. The FRF-data calculated at a total of 27 excitation frequencies are used to obtain the results shown in Figure 12. The 27 excitation frequencies are chosen within six different frequency ranges, i.e., the low-frequency range $0 < \omega < 500$ Hz, the mid-frequency range $500 < \omega < 1000$ Hz, the high frequency range $1{,}000 < \omega < 1{,}500$ Hz, and so forth. Figure 12 shows that the accuracy of damage identification becomes relatively poor (in other words, DIE has relatively high value) when the FRF-data at high frequencies are used for damage identification. For the tested beam specimen, the best damage

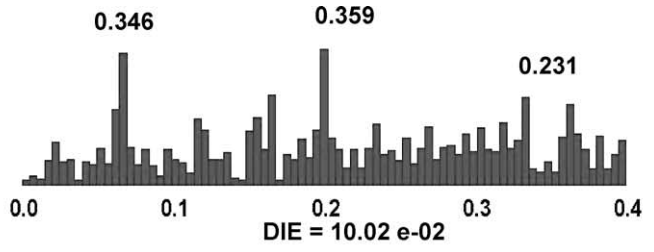

(a) FRF measurement points : x = 0.044, 0.069, 0.089 m

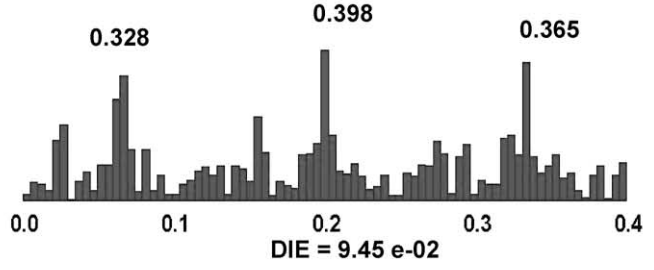

(b) FRF measurement points : x = 0.178, 0.202, 0.222 m

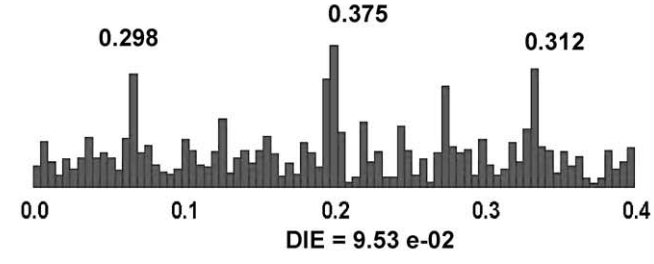

(c) FRF measurement points : x = 0.311, 0.336, 0.355 m

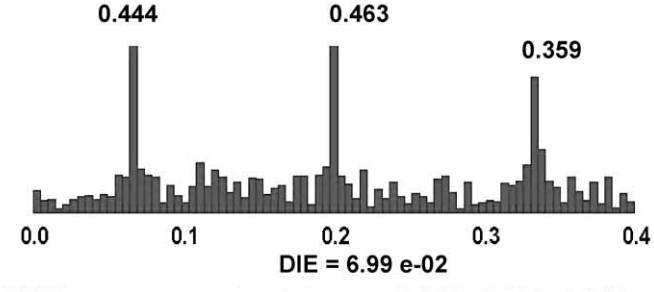

(d) FRF measurement points : x = 0.089, 0.202, 0.311 m

Figure 13. Experimentally measured FRF-data-based damage identification results depending on the FRF measurement points.

identification results are obtained when the FRF-data at both low and mid frequencies are used.

Figure 13 is given to show the effects of FRF measurement points on the accuracy of damage identification. Comparison is made for four different sets of FRF measurement points. Each set consists of three FRF measurement points chosen from the area near the

root of the beam specimen for the first set (Figure 13(a)), from the mid area for the second set (Figure 13(b)), and from the area near the free end (Figure 13(c)). The last set (Figure 13(d)) consists of points each from the areas near the root, mid, and free end of the beam specimen. Figure 13 shows that the last set provides the best damage prediction in terms of DIE while the other sets provide relatively poor results. Because the accelerometer is less sensitive in nature to measure the small vibration near the root, Figure 13(a) shows that the first set fails to successfully locate the damage near the free end. To obtain improved damage identification results by using the FRFs measured by the accelerometer, the FRF measurement points should not all be chosen in a narrow area and the points where the accelerometer will work poorly should not be considered.

5. CONCLUSIONS

Motivated by the advantages of FRF-data and the exact dynamic stiffness matrix, a frequency-domain method of structural damage identification is derived from the dynamic stiffness equation of motion of a structure and then applied to a beam structure. In the present SDIM, only the FRF-data measured from the damaged structure are required as the input data. The feasibility of the present SDIM is evaluated through some numerically simulated damage identification tests. Experiments are then conducted for the cantilevered beam with damage caused by introducing three slots of different depths to verify the present SDIM. It is shown that the present SDIM fairly well locates and quantifies the damage (i.e., the three slots) when the experimentally measured FRFs are used as the input data.

ACKNOWLEDGMENTS

This work was supported by Korea Research Foundation Grant. KRF-2001-041-E00034.

REFERENCES

1. R. D. Adams, P. Cawley, C. J. Pye and B. J. Stone 1978 *Journal of Mechanical Engineering Science* **20**, 93–100. A vibration technique for non-destructively assessing the integrity of structures.
2. C. Cempel, H. G. Matkem and A. Ziolkowski 1992 in *Structural Integrity Assessment* (P. Stanley, editor), 246–255. Oxford: Elsevier. Application of transformed normal modes for damage location in structures.
3. S. F. Griffin and C. T. Sun 1991 *Proceedings of the 28th Annual Technical Meeting of SES*. Health monitoring of dumb and smart structures.
4. P. Cornwell, S. W. Doebling and C. R. Farrar 1999 *Journal of Sound and Vibration* **224**, 359–374. Application of the strain energy damage detection method to plate-like structures.
5. J. S. Lew 1995 *AIAA Journal* **33**, 2189–2193. Using transfer function parameter changes for damage detection of structures.
6. A. K. Pandey and M. Biswas 1995 *International Journal of Analytical and Experimental Modal Analysis* **10**, 104–117. Damage diagnosis of truss structures by estimation of flexibility change.
7. J. M. Ricles and J. B. Kosmatka 1992 *AIAA Journal* **30**, 2310–2316. Damage detection in elastic structures using vibratory residual forces and weighted sensitivity.
8. K. T. Feroz and S. O. Oyadiji 1999 *Proceedings of the* 1999 *ASME Design Engineering Technical Conferences, Las Vegas, NV, DETC*99/*VIB*-8372. Damage detection in rods using wave propagation and regression analysis.
9. B. S. Wong, T. C. Guan and L. M. King 1993 *British Journal of NDT* **35**, 3–9. Mechanical impedance inspection of composite structures.

10. S. K. THYAGARAJAN, M. J. SCHULZ and P. F. PAI 1998 *Journal of Sound and Vibration* **210**, 162–170. Detecting structural damage using frequency response functions.
11. H. T. BANKS, D. J. INMAN, D. J. LEO and Y. WANG 1996 *Journal of Sound and Vibration* **191**, 859–880. An experimentally validated damage detection theory in smart structures.
12. Z. WANG, R. M. LIN and M. K. LIM 1997 *Computer Methods in Applied Mechanics and Engineering* **147**, 187–197. Structural damage detection using measured FRF data.
13. J. F. DOYLE 1997 *Wave Propagation in Structures*: *Spectral Analysis Using Fast Discrete Fourier Transforms*. New York: Springer-Verlag.
14. U. LEE, J. KIM and A. Y. T. LEUNG 2000 *The Shock and Vibration Digest* **32**, 451–465. The spectral element method in structural dynamics.
15. D. J. EWINS 1984 *Modal Testing*: *Theory and Practice*. Hertfordshire: Research Studies Press Ltd.
16. M. M. F. YUEN 1985 *Journal of Sound and Vibration* **103**, 301–310. A numerical study of the eigenparameters of a damaged cantilever.
17. H. LUO and S. HANAGUD 1997 *International Journal of Solids and Structures* **34**, 4557–4579. An integral equation for changes in the structural dynamics characteristics of damaged structures.
18. J. N. REDDY 1993 *An Introduction to the Finite Element Method*. New York: McGraw-Hill.
19. U. LEE and J. SHIN 2002 *Computers & Structures* **80**, 117–132. A frequency response function-based structural damage identification method.